DALTON
FULL PAPER

# Metal complexes of dipyridine hexaaza macrocycles. Structural differences between 18- and 20-membered macrocycles on complexation †

**Luís Branco,[a] Judite Costa,[a,b] Rita Delgado,[a,c] Michael G. B. Drew,[d] Vítor Félix [c] and Brian J. Goodfellow [e]**

[a] *Instituto de Tecnologia Química e Biológica, UNL, Apartado 127, 2781-901 Oeiras, Portugal*
[b] *Faculdade de Farmácia de Lisboa, Av. das Forças Armadas, 1600 Lisboa, Portugal*
[c] *Instituto Superior Técnico, Av. Rovisco Pais, 1049-001 Lisboa, Portugal*
[d] *Department of Chemistry, University of Reading, Whiteknights, Reading, UK RG6 6AD*
[e] *Departamento de Química, Universidade de Aveiro, 3810-193 Aveiro, Portugal*

***Received 30th April 2002, Accepted 15th July 2002***
***First published as an Advance Article on the web 23rd August 2002***

The hexaaza macrocycles 3,6,14,17,23,24-hexaazatricyclo[17.3.1.1$^{8,12}$]tetracosa-1(23),8,10,12(24),19,21-hexaene ([18]py$_2$N$_4$) and 3,7,15,19,25,26-hexaazatricyclo[19.3.1.1$^{9,13}$]hexacosa-1(25),9,11,13(26),21,23-hexaene ([20]py$_2$N$_4$) were synthesised. The protonation constants of both compounds and the stability constants of their complexes with a wide range of metal ions ($Mn^{2+}$, $Ni^{2+}$, $Cu^{2+}$, $Zn^{2+}$, $Cd^{2+}$, $Pb^{2+}$, $Mg^{2+}$, $Ca^{2+}$, $Ba^{2+}$, $La^{3+}$ and $Gd^{3+}$) were determined at 25 °C with ionic strengths of 0.10 mol dm$^{-3}$ in $KNO_3$. The overall basicity of [20]py$_2$N$_4$ is 3.20 log units larger than that of [18]py$_2$N$_4$ due to the weaker repulsion between the contiguous protonated ammonium sites, which are separated by propyl chains in [20]py$_2$N$_4$ rather than ethyl chains in [18]py$_2$N$_4$. The stability constants of complexes of each metal decrease as the cavity size of the macrocycle is increased, taking into account the difference in basicity of the ligands; the values for the $Cu^{2+}$, $Ni^{2+}$ and $Zn^{2+}$ complexes of both ligands are exceptionally high. Single crystal structures of complexes [Ni([18]py$_2$N$_4$)](ClO$_4$)$_2$·2CH$_3$CN (**1**), [Cu([18]py$_2$N$_4$)](ClO$_4$)$_2$·2CH$_3$CN (**2**), [Co([20]py$_2$N$_4$)]-[Co(H$_2$O)$_6$]$_{0.5}$(SO$_4$)$_2$·CH$_3$OH·4H$_2$O (**3**), [Ni([20]py$_2$N$_4$)](ClO$_4$)$_2$(**4**) and [Cu([20]py$_2$N$_4$)](ClO$_4$)$_2$ (**5**) were determined. In all complexes, the metal centre exhibit a hexaco-ordinate environment and the macrocycle adopts a twisted helical topology. The effect of the cage sizes of [18]py$_2$N$_4$ and [20]py$_2$N$_4$ on the molecular dimensions of metal complexes of both macrocycles is evaluated and a significant decrease in the helicity is observed in complexes of the 18-membered macrocycle compared to complexes of the 20-membered ring. The X-ray structural results, together with molecular mechanics calculations and NMR studies performed for metal complexes of both macrocycles, indicate that both ligands have enough flexibility to encapsulate smaller and larger metal ions, although it is clear that [20]py$_2$N$_4$ is more flexible than [18]py$_2$N$_4$.

## Introduction

Hexaaza macrocycles exhibit interesting co-ordination properties, being capable of forming both mononuclear and dinuclear complexes.[1] In the mononuclear complexes, they can encapsulate metals in an octahedral geometry, giving facial or meridional topological arrangements.[2] In dinuclear complexes, each metal is co-ordinated to three amine nitrogen atoms of the macrocycle. Metal co-ordination is completed by solvent molecules or a single or double bridging molecule or ion between the two metal ions; bridging ligands are normally added during synthesis for this purpose.[1,3,4] However, dinuclear complexes of 18- or 20-membered hexaazamacrocycles are rare,[5,6] the tendency of these species to form increases as the chain length between the two triamine moieties increases.

Changing two of the amines of the hexaaza macrocycle to aromatic nitrogen groups, *e.g.* pyridine rings, leads to significant structural changes on metal co-ordination. The 18-membered ligands ([18]py$_2$N$_4$ and Me$_4$[18]py$_2$N$_4$, see Scheme 1) can encapsulate metal ions with octahedral geometry only in a meridional mode, due to the rigidity imposed by the pyridine rings. A double helix around the metal is formed, with each strand starting at the methylenic group close to one pyridine (py–CH$_2$N–) and finishing at the corresponding group of the other pyridine ring.[7–10] Only one of the five possible NH isomers of [18]py$_2$N$_4$ or Me$_4$[18]py$_2$N$_4$ is able to twist around the metal, producing an octahedral *mer* complex having $D_2$ symmetry, which corresponds to *R*,*R*,*R*,*R* or *S*,*S*,*S*,*S* chirality. Two enantiomers are formed, each one twisting in only one direction, giving two different helical topologies, Λ and Δ.[7–10]

The aim of the present work is to understand the effect of the increase in cavity size on the stability and conformation of 18- to 20-membered hexaaza macrocycles containing two pyridine rings ([18]py$_2$N$_4$ and [20]py$_2$N$_4$) in metal complexes. Thus, we need to investigate whether the ligand [20]py$_2$N$_4$ can encapsulate metal ions, forming octahedral complexes, and to establish whether it adopts planar conformations in complexes with large metal ions. The ligand [18]py$_2$N$_4$ and some of its complexes have already been studied,[8–12] however, much less work has been carried out with [20]py$_2$N$_4$.[11,13] To the best of our knowledge, no crystal structures or any structural studies in solution of complexes of [20]py$_2$N$_4$ are known.[14]

To accomplish our aims some work already carried out on [18]py$_2$N$_4$ has been repeated and extended to [20]py$_2$N$_4$ under the same conditions, for comparison. The determination of stability constants of both ligands with several metal ions,

† Electronic supplementary information (ESI) available: plot of steric energy *versus* M–N$_{sp^3}$ distance for [M([*x*]py$_2$N$_4$)]$^{n+}$ (Fig. S1), NMR spectrum of [Zn([18]py$_2$N$_4$)]$^{2+}$ (Fig. S2) and table of RMS deviations obtained with fitting of the atomic positions of the [*x*]py$_2$N$_4$ framework in complexes **1**–**9** (Table S1). See http://www.rsc.org/suppdata/dt/b2/b204189h/

DOI: 10.1039/b204189h

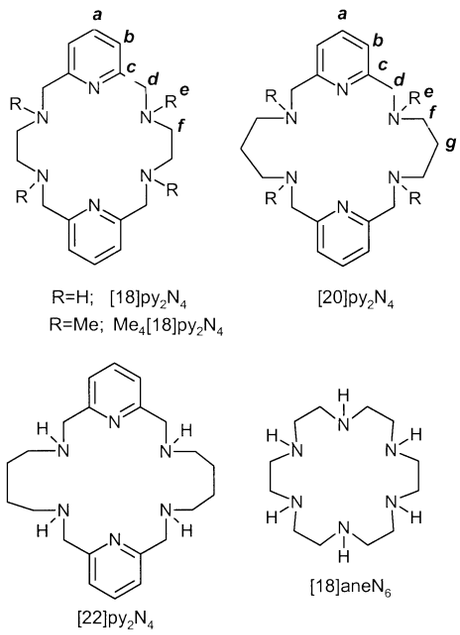


**Scheme 1**

together with structural studies in solution of diamagnetic complexes by NMR spectroscopy and of other complexes by X-ray single crystal diffraction have allowed a complete understanding of the behaviour of both ligands.

## Results and discussion

### Synthesis of macrocycles

Compounds $[18]py_2N_4$ and $[20]py_2N_4$ were prepared in good yield by [2 + 2] condensation of 2,6-pyridinedicarbaldehyde and ethylenediamine or propylenediamine, respectively, using $Ba^{2+}$ as the template ion, followed by the reduction of the resulting tetraimines.[8,13] Previously, pure compounds were obtained as salts by precipitation of the tetraprotonated bromide, $H_4([18]py_2N_4)Br_4$,[8] or chloride, $H_4[20]py_2N_4Cl_4$,[13] but in our case, pure cyclic amines were obtained as powders and used in this form.

### Acid–base behaviour and metal complex studies

The acid–base reactions of $[18]py_2N_4$ and $[20]py_2N_4$ and their stability constants with several divalent metal ions have been studied by potentiometric and/or spectrophotometric methods. The results are collected in Table 1, together with the stability constants of $[22]py_2N_4$ and $[18]aneN_6$, for comparison. The values for the protonation constants are similar to those published by Herman *et al.*,[11] except that we have also determined $\log K_5^H$ for $[18]py_2N_4$. The compound $[18]py_2N_4$ has the lowest overall basicity due to the stronger repulsion of consecutive positive protonated amine centres separated by ethyl chains, as opposed to the propyl chains of $[20]py_2N_4$, resulting in $\log K_3^H$ and $\log K_4^H$ values that are significantly larger for this ligand (see Table 1). $[22]py_2N_4$, which has n-butyl chains between consecutive amines, would be expected to have even higher basicity, but the published data do not confirm this.[15]

The stability constants were determined with most of the first transition metal ions, together with $Cd^{2+}$ and $Pb^{2+}$, some alkaline earths ($Mg^{2+}$, $Ca^{2+}$ and $Ba^{2+}$) and some lanthanides in the case of $[20]py_2N_4$. The complexes of $Co^{2+}$ with both ligands were impossible to study due to their fast oxidation, even when working in inert media. The $Ag^+$ complexes also undergo fast decomposition, with the formation of $Ag^0$, and a colour change of the solutions from colourless to pink. The stability constants for the complexes formed with the alkaline earth metal ions are very low, as expected for amine compounds. Accurate values for the $Mg^{2+}$ complexes of both ligands and for $Ba^{2+}$ with $[20]py_2N_4$ were impossible to obtain by the methods used, as they were very low.

In all cases, only mononuclear complexes of the type ML, MHL and ML(OH) were formed, see Table 1. The ML(OH) species was accurately determined only in a few cases, because precipitation usually occurs in the pH range within which it is formed. When it was determined with only a few experimental points, the values are given in parenthesis in Table 1. We checked for the possible formation of dinuclear $M_2L$ complexes, but it appears that they are not formed in aqueous solution under our conditions. Special attention was paid to the formation of $[Cu_2([20]py_2N_4)]^{4+}$, for which a stability constant has been published.[11] This species is chemically expected and it has been found by EPR spectroscopy and its crystal X-ray structure determined.[16] However, in this work, the $[Cu_2([20]py_2N_4)]^{4+}$ species could not be detected, either from potentiometric or spectrophotometric data. These data resulted from a collection of experimental titrations performed for 1 : 1 and 2 : 1 ratio (metal : ligand) solutions and treated together with the Hyperquad program.[17] For the $Cu^{2+}$–$[20]py_2N_4$ system, the results are listed in Table 2 for the two best models tested, along with the respective statistical parameters from the program. These results show that the model that includes the $MH_2L$ species converges with better statistical parameters than the model including the $M_2L$ species.

Although most of the stability constants have already been published,[8,11] we have extended the determinations to the complexes of $[20]py_2N_4$ with $Mn^{2+}$, together with some alkaline earth and lanthanide ions. The values of $\log K_{ML}$ determined in this work are lower than those published.[11] In general, only minor differences in the values were found, except for the nickel complexes of both ligands and for the copper complex of $[18]py_2N_4$, for which larger differences were observed. Our selected models also include MHL and, in certain cases, the $MH_2L$ and ML(OH) species. Larger differences were found when comparing our values with those of Jackels *et al.*,[8] and these are higher than expected, even when taking into account the different experimental conditions.

Our values for the $Ni^{2+}$ and $Cu^{2+}$ complexes were determined by potentiometry, in different M : L ratios, and re-determined by spectrophotometric techniques. For the $Cu^{2+}$ complexes, a batch method was used, with data reading 15 days after preparation of the solutions and confirmed after a further 15 days. For the complexes of $[20]py_2N_4$, the same values for the constants, and the same model, were obtained using the values from either technique, or both combined, which is a clear indication that the complex formation is sufficiently fast to be performed by automated methods. For $[18]py_2N_4$, the stability constants with those metal ions could not be obtained by potentiometric data alone, because the complexes are almost completely formed at low pH, and so the spectrophotometric data were essential for the determinations.

The stability constants of complexes of each metal decrease as the cavity size of the macrocycle increases ($[18]py_2N_4$ > $[20]py_2N_4$ > $[22]py_2N_4$[15]), taking into account the difference in basicity of the ligands by using the determined pM values at pH = 7.0. The decrease in the pM values is only slightly larger between $[20]py_2N_4$ and $[22]py_2N_4$ ($\Delta_{2-3}$) than between the first two ligands ($\Delta_{1-2}$), except for the $Ni^{2+}$ complexes, where $\Delta_{2-3}$ is very high, and for the $Pb^{2+}$ complexes, where the reverse occurs. For each ligand, the Irving–Williams order of stability is followed: $Mn^{2+} < Ni^{2+} < Cu^{2+} >> Zn^{2+}$. The values for the other complexes follow the trend $Zn^{2+} > Cd^{2+} >>> Pb^{2+}$.

The stability constants of the $Ni^{2+}$, $Cu^{2+}$ and $Zn^{2+}$ complexes of $[18]py_2N_4$ and $[20]py_2N_4$ are so high when compared with linear hexaaza ligands[18] that octahedral environments of preorganised ligands are expected, as already found for

**Table 1** Protonation (log $K^{H}_{i}$) constants of [18]$py_2N_4$, [20]$py_2N_4$, [22]$py_2N_4$ and [18]$aneN_6$, and stability constants (log $K_{M_mH_hL_l}$) of their complexes with several divalent metal ions.[a] $T$ = 25.0 °C; $I$ = 0.10 mol $dm^{-3}$ in $KNO_3$

| Ion | Equilibrium quotient | [18]$py_2N_4$ | | [20]$py_2N_4$ | | [22]$py_2N_4$[b] | [18]$aneN_6$ |
|---|---|---|---|---|---|---|---|
| $H^+$ | [HL]/[L] × [H] | 8.99(2) | 9.13[c]; 8.99[d] | 9.38(1) | 9.35[d] | 9.11 | 10.19[e]; 10.42[f] |
| | $[H_2L]/[HL] \times [H]$ | 8.22(2) | 8.32[c]; 8.16[d] | 8.61(1) | 8.73[d] | 8.32 | 9.23[e]; 9.58[f] |
| | $[H_3L]/[H_2L] \times [H]$ | 6.03(2) | 6.12[c]; 5.97[d] | 7.35(1) | 7.36[d] | 7.12 | 8.73[e]; 8.51[f] |
| | $[H_4L]/[H_3L] \times [H]$ | 5.34(3) | 5.24[c]; 5.20[d] | 6.44(2) | 6.59[d] | 3.72 | 4.09[e]; 4.89[f] |
| | $[H_5L]/[H_4L] \times [H]$ | 2.11(4) | — | — | — | — | 2[e]; 3[f] |
| | $[H_4L]/[L] \times [H]^4$ | 28.58 | 28.81[c]; 28.32[d] | 31.78 | 32.03[d] | 28.27 | 32.24[e]; 33.40[f] |
| $Ca^{2+}$ | [ML]/[M] × [L] | — | 4.4[c] | 1.8(1) | — | — | 2.5[e] |
| | [ML]/[MLOH] × [H] | — | — | 10.7(1) | — | — | — |
| $Ba^{2+}$ | [ML]/[M] × [L] | 1.9(1) | — | — | — | — | — |
| | [ML]/[MLOH] × [H] | 8.73(1) | — | — | — | — | — |
| $Mn^{2+}$ | [ML]/[M] × [L] | 11.79(2) | 12.5[c] | 8.22(2) | — | — | 10.50[g] |
| | [MHL]/[ML] × [H] | 5.11(4) | — | — | — | — | — |
| | [ML]/[MLOH] × [H] | (9.1) | — | 10.15(6) | — | — | — |
| $Co^{2+}$ | [ML]/[M] × [L] | — | — | — | — | 7.36 | 18.9[e] |
| | [MHL]/[ML] × [H] | — | — | — | — | — | 3.1[e] |
| | [ML]/[MLOH] × [H] | — | — | — | — | 8.1 | — |
| $Ni^{2+}$ | [ML]/[M] × [L] | 22.75(2) | 23.8[d] | 20.31(1) | 21.0[d] | 9.40 | 19.6[e] |
| | [MHL]/[ML] × [H] | 3.44(3) | — | 3.41(4) | — | — | 4.5[e] |
| $Cu^{2+}$ | [ML]/[M] × [L] | 24.72(3) | 25.9[d] | 21.13(1) | 21.30[d] | 12.83 | 24.40[g] |
| | [MHL]/[ML] × [H] | 2.28(4) | — | 5.12(2) | 5.01[d] | — | 3.00[g] |
| | $[MH_2L]/[MHL] \times [H]$ | — | — | 2.41(3) | — | — | 3.48[g] |
| | [ML]/[MLOH] × [H] | (9.7) | — | 10.12(2) | — | — | — |
| | $[M_2L]/[ML][M]$ | — | — | — | 4.9[d] | 5.7 | — |
| $Zn^{2+}$ | [ML]/[M] × [L] | 20.61(1) | 20.73[d] | 15.40(1) | 15.83[d] | 6.92 | 17.8[e]; 18.7[h] |
| | [MHL]/[ML] × [H] | 2.13(1) | — | 4.54(3) | — | — | —; 3.93[h] |
| | [ML]/[MLOH] × [H] | Precipitate | — | 9.75(4) | — | 7.33 | — |
| $Cd^{2+}$ | [ML]/[M] × [L] | 17.78(1) | 17.2[c]; 17.93[d] | 14.01(1) | 14.18[d] | 7.86 | 17.9[e]; 18.80[i] |
| | [MHL]/[ML] × [H] | 2.83(4) | — | 5.11(3) | — | — | — |
| | [ML]/[MLOH] × [H] | (9.6) | — | 10.41(5) | — | 7.51 | — |
| $Pb^{2+}$ | [ML]/[M] × [L] | 13.79(1) | 13.84[d] | 9.42(1) | 9.57[d] | 6.61 | 14.1[e]; 14.13[j] |
| | [MHL]/[ML] × [H] | 4.15(4) | — | 6.59(2) | — | — | —; 5.73[j] |
| | [ML]/[MLOH] × [H] | (9.3) | — | 10.14(3) | — | 8.07 | — |
| $La^{3+}$ | [ML]/[M] × [L] | — | 7.4[c] | 4.68(1) | — | — | 5.7[k]; 9.1[f] |
| | [ML]/[MLOH] × [H] | — | — | 9.18(3) | — | — | — |
| $Gd^{3+}$ | [ML]/[M] × [L] | — | 8.1[c] | 5.89(2) | — | — | 8.4[k]; 9.8[f] |
| $Sm^{3+}$ | [ML]/[M] × [L] | — | — | 5.57(2) | — | — | 8.14[k]; 10.1[f] |

[a] Values in parenthesis are standard deviations in the last significant figure. [b] 0.01 mol $dm^{-3}$ $NaClO_4$, ref. 15. [c] 0.2 mol $dm^{-3}$ KCl, ref. 8. [d] 0.1 mol $dm^{-3}$ $KNO_3$, ref. 11. [e] 0.20 mol $dm^{-3}$ $NaNO_3$, ref. 19. [f] 20 °C, 0.1 mol $dm^{-3}$ NaCl, ref. 20. [g] 0.15 mol $dm^{-3}$ $NaClO_4$, ref. 21. [h] 0.15 mol $dm^{-3}$ $NaClO_4$, ref. 22. [i] 0.15 mol $dm^{-3}$ $NaClO_4$, ref. 23. [j] 0.15 mol $dm^{-3}$ $NaClO_4$, ref. 24. [k] 0.20 mol $dm^{-3}$ $NaNO_3$, ref. 25.

**Table 2** Results of two different models obtained with the HYPERQUAD program[17] from experimental data of titrations of 1 : 1 and 2 : 1 mixtures of $Cu^{2+}$ and [20]$py_2N_4$

| Model[a] | Log $\beta_{M_mH_hL_l}$ | $\sigma$ | $\chi^2$ |
|---|---|---|---|
| [ML]/[M] × [L] | 21.13(1) | 1.8649 | 12.93 |
| [MHL]/[ML] × [H] | 26.25(2) | | |
| $[MH_2L]/[MHL] \times [H]$ | 28.66(2) | | |
| [ML]/[MLOH] × [H] | 11.01(2) | | |
| [ML]/[M] × [L] | 20.99(3) | 3.5017 | 38.67 |
| [MHL]/[ML] × [H] | 26.10(1) | | |
| $[M_2L]/[ML][M]$ | 25.93(5) | | |
| [ML]/[MLOH] × [H] | 10.87(4) | | |

[a] Where L is [20]$py_2N_4$ and M is $Cu^{2+}$.

$[Zn([18]py_2N_4)]^{2+}$,[9] $[Cd([18]py_2N_4)]^{2+}$,[10] $[Co(Me_4[18]py_2N_4)]^{2+}$ [7] and $[Cu(Me_4[18]py_2N_4)]^{2+}$.[7] The values of $K_{ML}$ for [18]$py_2N_4$ are also larger than those of the corresponding complexes of [18]$aneN_6$,[19–25] (see Table 1), taking into account the different basicity of the ligands. Indeed, the stability constants of metal complexes of ligands containing pyridine tend to be higher than would be predicted on the basis of the weak σ-donating properties of the pyridine nitrogen atoms, if it can be assumed that the protonation constants of the ligand reflect this ability.[26] As already observed for other macrocycles containing pyridine,[26,27] the $Co^{2+}$ complex of [18]$py_2N_4$ (and also of [20]$py_2N_4$) is not stable, while that of [18]$aneN_6$ is stable enough to allow the determination of its stability constant.

## Structural studies

### Single crystal X-ray structures

The solid state structures of hexaaza macrocycle complexes $[Ni([18]py_2N_4)](ClO_4)_2 \cdot 2CH_3CN$ (**1**), $[Cu([18]py_2N_4)](ClO_4)_2 \cdot 2CH_3CN$ (**2**), $[Co([20]py_2N_4)][Co(H_2O)_6]_{0.5}(SO_4)_2 \cdot CH_3OH \cdot 4H_2O$ (**3**), $[Ni([20]py_2N_4)](ClO_4)_2$ (**4**) and $[Cu([20]py_2N_4)](ClO_4)_2$ (**5**) were determined using single crystal X-ray diffraction.

The crystal structures of **1** and **2**, built up in the space group *C*2/*c*, contain three crystallographically independent species: one $ClO_4^-$, one $CH_3CN$ solvent molecule and one complex cation; $[Ni([18]py_2N_4)]^{2+}$ in **1** and $[Cu([18]py_2N_4)]^{2+}$ in **2**. In both cases, the solvent and the counter anion are located on general positions in the crystal lattice, while the complex cation is positioned on the twofold crystallographic axis, leading to the molecular formula $[M([18]py_2N_4)](ClO_4)_2 \cdot 2CH_3CN$ (M = $Ni^{2+}$ or $Cu^{2+}$). The complexes **1** and **2** display similar unit cell dimensions (see Table 3) and comparable molecular dimensions subtended at metal centres, suggesting that they are isomorphous. In fact, the match between the non-hydrogen atomic coordinates of the complex cations **1** and **2** gives root mean square deviations (RMS) of only 0.059 Å. The molecular structure and the equivalent atomic notation scheme used are shown in Fig. 1(a) for $[Ni([18]py_2N_4)]^{2+}$ (**1**) and in Fig. 1(b) for $[Cu([18]py_2N_4)]^{2+}$ (**2**). In both complexes, the metal centre is encapsulated by the macrocycle in a hexaco-ordinate environment. The macrocycle is twisted in a helical topology, leading to the formation of two meridional linkages containing the pyridine nitrogen atom and two adjacent aliphatic amines. The twisting

**Table 3** Room temperature crystal data and pertinent refinement details for complexes **1**–**5**

| Complex | **1** | **2** | **3** | **4** | **5** |
|---|---|---|---|---|---|
| Molecular formula [a] | $[NiL^1](ClO_4)_2\cdot 2CH_3CN$ | $[CuL^1](ClO_4)_2\cdot 2CH_3CN$ | $[CoL^2][Co(H_2O)_6]_{0.5}(SO_4)_2\cdot 4H_2O\cdot MeOH$ | $[NiL^2](ClO_4)_2$ | $[CuL^2](ClO_4)_2$ |
| Empirical formula | $C_{22}H_{32}Cl_2N_8NiO_8$ | $C_{22}H_{32}Cl_2CuN_8O_8$ | $C_{21}H_{48}Co_{1.5}N_6O_{16}S_2$ | $C_{20}H_{30}Cl_2N_6NiO_8$ | $C_{20}H_{30}Cl_2CuN_6O_8$ |
| $M_w$ | 666.17 | 671.00 | 793.17 | 612.11 | 616.94 |
| Crystal system | Monoclinic | Monoclinic | Orthorhombic | Monoclinic | Monoclinic |
| Space group | *C*2/*c* | *C*2/*c* | *Pnn*2 | $P2_1/n$ | $P2_1/n$ |
| *a*/Å | 20.023(27) | 19.990(26) | 20.089(27) | 12.140(17) | 12.121(17) |
| *b*/Å | 15.041(18) | 15.012(16) | 16.349(20) | 13.478(18) | 13.534(18) |
| *c*/Å | 11.869(14) | 11.921(14) | 9.766(14) | 17.277(23) | 17.046(24) |
| *β*/° | 123.33(1) | 123.57(1) | (90) | 110.58(1) | 110.46(1) |
| *V*/Å$^3$ | 2987(6) | 2981(6) | 3207(7) | 2647(6) | 2620(6) |
| *Z* | 4 | 4 | 4 | 4 | 4 |
| $D_c$/Mg m$^{-3}$ | 1.482 | 1.495 | 1.643 | 1.536 | 1.564 |
| $\mu$/mm$^{-1}$ | 0.886 | 0.970 | 0.996 | 0.990 | 1.094 |
| Reflections collected | 4417 | 3161 | 7735 | 8505 | 8132 |
| Unique reflections [*R*(int)] | 2686 [0.0810] | 1899 [0.1740] | 3001 [0.1158] | 4578 [0.0938] | 4922 [0.0384] |
| $R_1$, $wR_2$ [$I > 2\sigma(I)$] | 0.0921, 0.2609 | 0.1134, 0.2791 | 0.0713, 0.1646 | 0.0811, 0.2094 | 0.0701, 0.1962 |
| $R_1$, $wR_2$ (all data) | 0.1461, 0.2981 | 0.1600, 0.3096 | 0.1347, 0.1870 | 0.1826, 0.2463 | 0.1030, 0.2183 |

[a] $L^1 = [18]py_2N_4$ and $L^2 = [20]py_2N_4$.

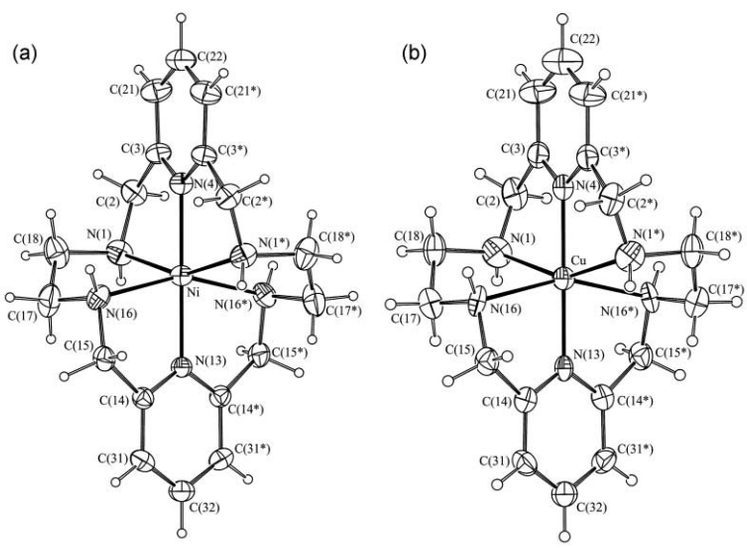


**Fig. 1** ORTEP views of $[18]py_2N_4$ complexes, showing the overall geometry of the *S*,*S*,*S*,*S* forms: (a) $[Ni([18]py_2N_4)]^{2+}$ (**1**) with ellipsoids drawn at 20% probability level; (b) $[Cu([18]py_2N_4)]^{2+}$ (**2**) with ellipsoids drawn at 30% probability level.

of the macrocycle, given by the angle between the two pyridine rings, is 73.6(4)° in **1** and 74.2(6)° in **2**. The bond distances and angles subtended at the metal centre are listed in Table 4 and indicate that the co-ordination geometries are pseudo-octahedral. Both molecules contain a twofold crystallographic axis running through the metal centre and the two axial pyridine nitrogen donors, giving an $N_{sp^2}$–M–$N_{sp^2}$ angle of 180° and four independent M–N bond distances: two M–$N_{sp^2}$ bonds of 2.034(8) and 2.024(7) Å in **1**, and 1.996(9) and 1.970(9) Å in **2**, and two M–$N_{sp^3}$ bonds of 2.153(7) and 2.164(7) Å in **1**, and 2.265(11) and 2.190(9) Å in **2**.

Complex **3** is built up from an asymmetric unit composed of two cationic species, one $[Co([20]py_2N_4)]^{3+}$ and one $[Co(H_2O)_6)]^{2+}$, two $SO_4^{2-}$ anions, and five crystallisation solvent molecules, one methanol and four water molecules. The complex $[Co(H_2O)_6)]^{2+}$ displays twofold crystallographic symmetry so that the complex as a whole has the molecular formula $[Co([20]py_2N_4)][Co(H_2O)_6)]_{0.5}(SO_4)_2\cdot CH_3OH\cdot 4H_2O$. The assignment of the cobalt oxidation sates in this compound is not trivial, since the charge balance requires the presence, in the unit cell, of two independent cobalt centres of different formal oxidation states, +3 and +2 respectively. The Co–$N_{sp^2}$ and Co–$N_{sp^3}$ bond distances in **3** are considerably shorter, by *ca.* 0.190 and 0.252 Å, respectively, than those found in the related complex $[Co(Me_4[18]py_2N_4)]^{2+}$ (**6**), in which the cobalt is in the oxidation state +2 and is surrounded by the six nitrogen donor atoms of the hexaaza macrocycle in a co-ordination environment comparable to that found for the $[18]py_2N_4$ complex

**Table 4** Selected bond lengths (Å) and angles (°) for 18-membered macrocyclic complexes **1** and **2**

| | **1** (M = $Ni^{2+}$) | **2** (M = $Cu^{2+}$) |
|---|---|---|
| M–N(4) | 2.034(8) | 1.996(9) |
| M–N(1) | 2.153(7) | 2.265(11) |
| M–N(13) | 2.024(7) | 1.970(9) |
| M–N(16) | 2.164(7) | 2.190(9) |
| N(13)–M–N(4) | 180.0 | 180.0 |
| N(1)–M–N(1)[a] | 154.7(4) | 153.1(4) |
| N(16)–M–N(16)[a] | 155.6(3) | 155.9(4) |
| N(4)–M–N(1) | 77.4(2) | 76.5(2) |
| N(13)–M–N(1) | 102.6(2) | 103.5(2) |
| N(13)–M–N(16) | 77.8(2) | 78.0(2) |
| N(1)–M–N(16) | 82.5(3) | 80.1(4) |
| N(4)–M–N(16) | 102.2(2) | 102.0(2) |
| N(1)–M–N(16)[a] | 102.8(3) | 105.6(4) |

[a] Denotes the symmetry operation: $-x + 1, y, -z + 3/2$.

**Table 5** Tetrahedral distortion and helicity parameters of hexaaza macrocyclic complexes of type $[M([x]py_2N_4)]^{n+}$ ($x$ = 18 or 20)

| Complex | Metal ion | Ionic radius/Å | Deviation of $N_{sp^3}$ from $N_4$ plane [a]/Å | | | | $N_{sp^3}$–M–$N_{sp^3}$ | $N_{sp^2}$–M–$N_{sp^2}$ | $\alpha$ [b]/° | $\beta$ [c]/° |
|---|---|---|---|---|---|---|---|---|---|---|
| | | | N(1) | N(2) | N(3) | N(4) | | | | |
| $[18]py_2N_4$ | | | | | | | | | | |
| **2** | $Cu^{2+}$ | 0.72 | −0.49(1) | 0.49(1) | −0.49(1) | 0.49(1) | 153.1(4), 155.9(4) | 180.0 | 74.2(6) | −106.2(7) |
| **1** | $Ni^{2+}$ | 0.78 | −0.46(1) | 0.46(1) | −0.46(1) | 0.46(1) | 154.7(4), 155.6(3) | 180.0 | 73.6(4) | −107.6(5) |
| **7** | $Zn^{2+}$ | 0.83 | −0.57 | 0.57 | −0.57 | 0.57 | 150.2(1), 150.2(1) | 180.0 | 74.5 | −105.1 |
| **8** | $Cd^{2+}$ | 1.03 | −0.76 | 0.75 | −0.75 | 0.76 | 142.9(2), 142.9(2) | 176.0(2) | 88.4 | −91.6 |
| $Me_4[18]py_2N_4$ | | | | | | | | | | |
| **9** | $Cu^{2+}$ | 0.72 | −0.48 | 0.48 | −0.49 | 0.48 | 155.1(2), 155.7(2) | 178.2(2) | 74.2 | −105.5 |
| **6** | $Co^{2+}$ | 0.82 | −0.51 | 0.50 | −0.51 | 0.52 | 153.5(2), 153.7(2) | 178.4(2) | 75.1 | −104.9 |
| $[20]py_2N_4$ | | | | | | | | | | |
| **3** | $Co^{3+}$ | 0.64 | −0.20(1) | 0.20(1) | −0.20(1) | 0.20(1) | 168.8(5), 168.1(5) | 177.8(4) | 84.9(3) | −93.6(11) |
| **5** | $Cu^{2+}$ | 0.72 | −0.46(1) | 0.47(1) | −0.45(1) | 0.49(1) | 160.0(2), 150.6 (2) | 172.2(2) | 64.3(2) | −115.0(5) |
| **4** | $Ni^{2+}$ | 0.78 | −0.43(1) | 0.43(1) | −0.45(1) | 0.45(1) | 158.8(3), 154.7(3) | 173.2(2) | 64.5(3) | −115.3(7) |

[a] Deviation of $N_{sp^3}$ from least-squares $N_4$ equatorial co-ordination plane. N(1) *trans* to N(3) and N(2) *trans* to N(4); (+) above the plane, (−) below the plane. [b] $\alpha$ is the angle between the pyridine rings. [c] $\beta$ is defined in the text and the quoted values correspond to the *S*,*S*,*S*,*S* configuration.

reported here. Apart from electronic and steric constraints, the differences found for the bond lengths Co–$N_{sp^2}$ and Co–$N_{sp^3}$ in **6** and **3** reflect the difference in the ionic radii of $Co^{2+}$ and $Co^{3+}$ (0.18 Å, see Table 5). This structural comparison unequivocally confirms the assignment of the +3 oxidation state for cobalt in $[Co([20]py_2N_4)]^{3+}$ and +2 in $[Co(H_2O)_6)]^{2+}$. Furthermore, complex **3** was prepared from the starting material $CoSO_4 \cdot 7H_2O$, and oxidation readily occurred in the presence of $[20]py_2N_4$, as reported above.

The crystal structures of **4** and **5** consist of $ClO_4^-$ anions and complex cations $[Ni([20]py_2N_4)]^{2+}$ (**4**) and $[Cu([20]py_2N_4)]^{2+}$ (**5**). Comparison of the unit cell dimensions (see Table 3) of **4** and **5** suggests that these two complexes are isomorphous, as also found for the corresponding complexes of the 18-membered macrocycle. However, these two complexes exhibit some significantly different M–N distances (see Table 6). On the other hand, the fitting of these two structures gives a RMS deviation in the atomic co-ordinates of the non-hydrogen atoms of $[20]py_2N_4$ of only 0.089 Å.

Molecular diagrams showing the overall geometry and the atomic labelling adopted are presented in Fig. 2 for $[Co([20]py_2N_4)]^{3+}$ (**3**) and in Fig. 3(a) and (b) for $[Ni([20]py_2N_4)]^{2+}$ (**4**) and $[Cu([20]py_2N_4)]^{2+}$ (**5**), respectively. In each structure, the metal centre is encapsulated by the macrocycle $[20]py_2N_4$ in

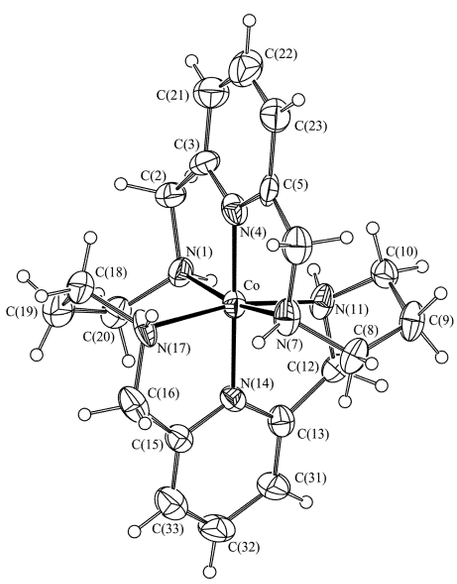


**Fig. 2** ORTEP view of $[Co([20]py_2N_4)]^{3+}$ (**3**), showing the overall geometry of the *S*,*S*,*S*,*S* stereochemistry. The ellipsoids are drawn at 30% probability level.

a pseudo-octahedral environment with six independent M–N bond distances (see Table 6). The pyridine and aliphatic nitrogen atoms occupy identical positions in the metal co-ordination sphere to those found for $[18]py_2N_4$ complexes. The $[20]py_2N_4$ macrocycle also adopts a helical conformation, with a twist between the two pyridine rings of 84.9(3)° in **3**, only 64.5(3)° in **4** and 64.3(2)° in **5**. To the best of our knowledge, these three structures represent the first X-ray structural determinations of metal complexes of $[20]py_2N_4$. In fact, no structures were retrieved in a search on the Cambridge Structural Data Base [14] for $[20]py_2N_4$.

The solid state structures of the 18- and 20-membered hexaaza macrocyclic complexes determined here are compared in Table 5, along with structural data for other reported $[18]py_2N_4$ and $Me_4[18]py_2N_4$ complexes, $[M([18]py_2N_4)]^{2+}$ {M = $Zn^{2+}$ (**7**), $Cd^{2+}$ (**8**)} [9,10] and $[M(Me_4[18]py_2N_4)]^{2+}$ {M = $Co^{2+}$ (**6**), $Cu^{2+}$ (**9**)}.[7] These complexes also exhibit helical topologies involving the meridional biding of the two $-N_{py}C_{sp^2}CH_2NHCH_2CH_2CH_2NHCH_2C_{sp^2}N_{py}-$ linkages of the macrocycle to the metal ion. Comparison of the structural data of the 18- and 20-membered macrocyclic complexes allows the effect of the cavity size on the molecular dimensions of the metal co-ordination sphere to be assessed. Furthermore, knowledge of steric flexibility of these two ligands also allows evaluation of their real capability to encapsulate metal ions with different ionic sizes in a hexa-co-ordinate environment.

In all complexes for which data are collected in Table 5, the four M–$N_{sp^3}$ distances are longer than the two M–$N_{sp^2}$ bonds, following the typical pattern found for metal complexes incorporating a pyridine moiety.[28,29] The copper and nickel complexes of $[18]py_2N_4$ (**1** and **2**) and $[20]py_2N_4$ (**4** and **5**) exhibit comparable M–N distances. For example, the average M–$N_{sp^3}$ distances for **1** and **2** are only slightly longer (0.04 Å) than those found for **4** and **5**. Therefore, this comparison indicates that both macrocycles have enough flexibility to fold and encapsulate the metal centres in cages with a helical shape and the M–N distances are determined basically by the stereoelectronic requirements of the metal. In the cases of cobalt complexes **3** and **6**, as mentioned above, the differences between the Co–N bond lengths reflect the difference in ionic size between $Co^{3+}$ and $Co^{2+}$ rather than some constraint imposed by the cavity size of the 18- or 20-membered macrocyclic ligand.

A further insight into the flexibility of both macrocycles in encapsulating metal centres is provided by the degree of distortion of the metal co-ordination sphere in the $[M([x]py_2N_4)]^{n+}$ complexes, which can be evaluated by considering the tetrahedral distortion of each aliphatic nitrogen atom from the best least-squares plane defined through the equatorial co-

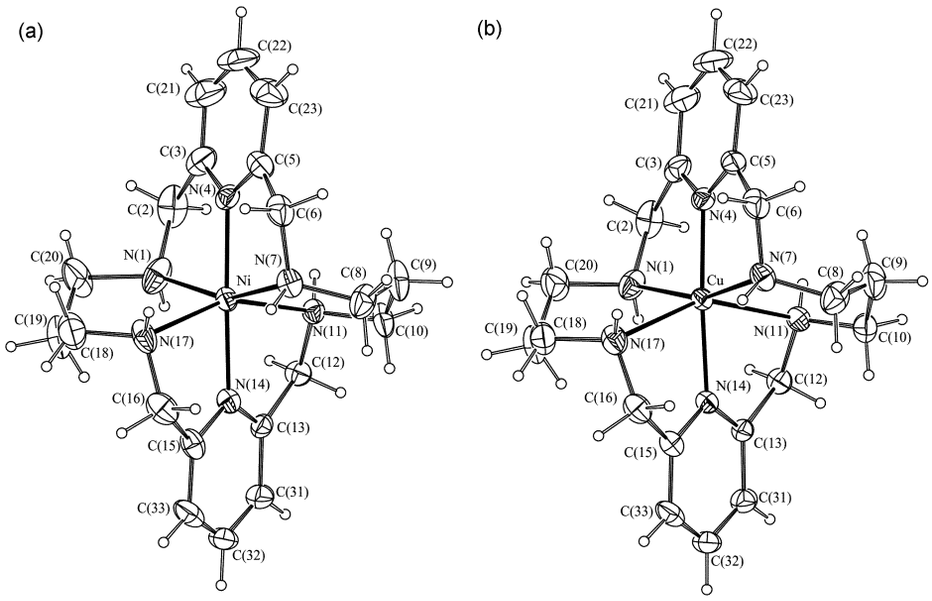


**Fig. 3** ORTEP views of $[20]py_2N_4$ complexes showing the overall geometry of the *S*,*S*,*S*,*S* forms of (a) $[Ni([20]py_2N_4)]^{2+}$ (**4**), with ellipsoids drawn at 30% probability level, and (b) $[Cu([20]py_2N_4)]^{2+}$ (**5**), with ellipsoids drawn at 20% probability level.

**Table 6** Selected bond lengths (Å) and angles (°) for 20-membered macrocyclic complexes **3**, **4** and **5**

| | **3** (M = $Co^{3+}$) | **4** (M = $Ni^{2+}$) | **5** (M = $Cu^{2+}$) |
|---|---|---|---|
| M–N(4) | 1.854(11) | 1.991(7) | 1.949(5) |
| M–N(14) | 1.871(10) | 2.006(6) | 2.017(5) |
| M–N(1) | 1.970(11) | 2.164(7) | 2.129(5) |
| M–N(11) | 1.973(10) | 2.189(5) | 2.341(5) |
| M–N(7) | 1.996(11) | 2.195(6) | 2.170(5) |
| M–N(17) | 2.008(10) | 2.229(6) | 2.411(5) |
| N(4)–M–N(14) | 177.8(4) | 173.2(2) | 172.2(2) |
| N(4)–M–N(1) | 83.2(5) | 79.7(3) | 80.9(2) |
| N(14)–M–N(1) | 94.7(5) | 96.3(3) | 96.1(2) |
| N(4)–M–N(11) | 95.4(5) | 97.1(2) | 97.3(2) |
| N(14)–M–N(11) | 84.0(5) | 77.5(2) | 75.8(2) |
| N(1)–M–N(11) | 90.4(5) | 92.5(2) | 96.0(2) |
| N(4)–M–N(7) | 85.7(5) | 79.7(3) | 80.4(2) |
| N(14)–M–N(7) | 96.5(5) | 104.7(2) | 103.3(2) |
| N(1)–M–N(7) | 168.8(5) | 158.8(3) | 160.0(2) |
| N(11)–M–N(7) | 91.6(4) | 94.9(2) | 93.3(2) |
| N(4)–M–N(17) | 96.5(5) | 108.1(3) | 111.7(2) |
| N(14)–M–N(17) | 84.0(5) | 77.5(3) | 75.5(2) |
| N(1)–M–N(17) | 91.1(5) | 94.2(3) | 93.5(2) |
| N(11)–M–N(17) | 168.1(5) | 154.7(3) | 150.6(2) |
| N(7)–M–N(17) | 89.2(5) | 87.4(2) | 86.9(2) |

ordination. For example, in the complex $[Ni([18]py_2N_4)]^{2+}$ (**1**), the nitrogen atoms N(16) and N(16*) of one meridional linkage lie 0.46(1) Å above the equatorial co-ordination plane [N(16), N(1),N(1*),N(16*)], while the nitrogens, N(1) and N(1*), of the other one are displaced −0.46(1) Å below the plane, leading to bending of the $Ni–N_{sp^3}$ bonds towards the pyridine rings, such that two different values of 154.7(4) and 155.6(3)° are observed for the *trans* $N_{sp^3}–Ni–N_{sp^3}$ chelating angles. The spanning of the two apparently rigid $–NCH_2C_{sp^2}N_{py}C_{sp^2}CH_2N–$ linkages is, undoubtedly, one of the causes of the tetrahedral distortion in this complex, as well as for the other structures for which values are quoted in Table 5. It is also evident from the structural data listed that for the incorporation of the metal ion by the macrocycle, a mechanism based on hole-size fitting involving the distortion of the co-ordination sphere occurs. In fact, for the $[18]py_2N_4$ complexes, including those of $Me_4[18]py_2N_4$, the extent of this tetrahedral distortion clearly reflects the metal ion size, following the order $Cd^{2+} > Zn^{2+} > Cu^{2+} > Ni^{2+}$. The $Cd^{2+}$ complex exhibits the largest tetrahedral distortion, since that this nucleus has the largest ionic radius (1.03 Å), while the smaller ions, $Cu^{2+}$ (0.72 Å) and $Ni^{2+}$ (0.78 Å), display considerably less distortion. Thus, the tetrahedral distortion exhibited in $[Co(Me_4[18]py_2N_4)]^{2+}$ (**6**) is expected when compared with that found in $[Ni([18]py_2N_4)]^{2+}$ (**1**), since $Co^{2+}$ (0.82 Å) is slightly larger than $Ni^{2+}$ (0.78 Å). The slightly larger distortions found in both copper complexes, $[Cu([18]py_2N_4)]^{2+}$ (**2**) and $[Cu(Me_4[18]py_2N_4)]^{2+}$ (**9**), unexpected only on the basis of the ionic radius of $Ni^{2+}$ and $Cu^{2+}$, are due to the Jahn–Teller effect. Indeed, the two $Cu–N_{sp^3}$ bond distances of 2.265(11) and 2.190(9) Å in **2** and 2.289(5) and 2.307(6) Å in **9** are significantly longer than the others. In other words, this electronic effect also contributes to the degree of tetrahedral distortion observed.

The same structural tendency is observed within the $[20]py_2N_4$ complexes. Indeed, the $Cu^{2+}$ and $Co^{3+}$ (0.64 Å) complexes display the largest and smallest tetrahedral distortions, respectively. The structural distortion data listed in Table 5 surprisingly show that ions with different ionic sizes, such as $Co^{3+}$, $Ni^{2+}$ or $Cu^{2+}$, fit more comfortably into the larger cages provided by $[20]py_2N_4$ than those formed by $[18]py_2N_4$, suggesting that the former is sterically more flexible than $[18]py_2N_4$. Therefore, it may also be expected that the 20-membered macrocycle is potentially more capable of encapsulating larger metal ions, such as $Pb^{2+}$ and $Cd^{2+}$, in a hexaco-ordinate environment than the 18-membered one. In order to check this assumption and to understand the co-ordination behaviour in solution of these two macrocycles towards metal ions of different ionic sizes, molecular mechanics calculations (MM) were carried out with the universal force field[30] within the Cerius[2] software, using a modelling methodology identical to that reported in our previous work.[28,29] Plots of the steric energy *versus* $M–N_{sp^3}$ distance for $[M([x]py_2N_4)]^{n+}$ ($x = 18$ or 20) complexes (Fig. S1, ESI) indicate that the two octahedral species have identical stabilities for smaller $M–N_{sp^3}$ distances up *ca.* 1.75 Å, while the complex $[M([20]py_2N_4)]^{n+}$ becomes the more stable at longer distances. Furthermore, the energy profiles of both curves have shallow energy minima at *ca.* 1.95 Å for $[M([18]py_2N_4)]^{n+}$ and *ca.* 2.00 Å for $[M([20]py_2N_4)]^{n+}$. The average $M–N_{sp^3}$ distances found for the $[18]py_2N_4$ complexes [2.158(7) Å in **1** and 2.228(9) Å in **2**] and for those of $[20]py_2N_4$ [1.987(10) Å in **3**, 2.194(6) Å in **4** and 2.263(5) Å in **5**] are within the valleys of the corresponding curve. These results, in spite of being for molecules in the gas phase, are perfectly consistent with the structural data and co-ordination behaviour described above for the complexes of these two ligands, *i.e.* the $[20]py_2N_4$ ligand has enough flexibility to form stable complexes either

with larger or smaller ions, such as $Co^{3+}$ or $Zn^{2+}$ and $Pb^{2+}$, respectively.

Table S1 (ESI) lists the RMS deviations obtained with the fitting of the atomic positions, excluding the hydrogen atoms, of the [18]$py_2N_4$ framework in complexes **1**, **2** and **6**–**9**, and of the [20]$py_2N_4$ framework in complexes **3**–**5**. The RMS values calculated for **1**, **2**, **6**, **7** and **9** are small (between 0.05 and 0.10 Å), indicating that the [18]$py_2N_4$ macrocycle adopts an identical helical topology in all these complexes. By contrast, the alignment of $Cd^{2+}$ complex **8** with each one of the other complexes, **1**, **2**, **6**, **7** and **9**, leads to larger RMS values (ranging from 0.26 to 0.34 Å), suggesting that the macrocycle distorts considerably in order to accommodate this larger metal ion, as mentioned above. Indeed, when the metal is removed from the [18]$py_2N_4$ cages of complexes **1**, **2**, **7** or **8** and then the structures optimised by MM using $Q_{eq}$ charges, the same conformation is obtained in all cases. The overlay between the [20]$py_2N_4$ in **3** *versus* **4** or **5** gives large RMS of 0.50 and 0.54 Å, respectively, showing that helical shape of the ligand in the cobalt complex is markedly different to those reported for **4** and **5**, because of the variation in chain length (see Table S1, ESI). Thus, the [20]$py_2N_4$ framework undergoes a structural change in order to provide a cage with the correct size to wrap the smaller $Co^{3+}$ ion. On the other hand, the helical conformation in cation **3** can also be affected by hydrogen bonds. In fact, the crystal structure of **3** shows the ions held together by a complex 3-D network of hydrogen bonds, involving N–H and C–H groups from the $[Co([20]py_2N_4)]^{3+}$ cation and the oxygen atoms of solvent water molecules, $SO_4^{2-}$ anions and the $[Co(H_2O)_6]^{2+}$ species. However, when the $Ni^{2+}$ is replaced by $Co^{3+}$ in complex **1** and the structure is subsequently minimised by MM, the resultant structure is identical to that obtained from the direct minimisation of **3**. This result clearly indicates that the hydrogen bonding interaction has a marginal effect on the macrocyclic conformation. Furthermore, the match between the X-ray structure and the structure optimised in the gas phase gives a somewhat large RMS of 0.19 Å.

As mentioned above, the co-ordination of the metal centre by the six nitrogen donor atoms of [18]$py_2N_4$ or [20]$py_2N_4$ in a meridional fashion gives rise to a pseudo-octahedral geometry with two types of chirality, namely Λ or Δ at the metal, and *R* or *S* at the nitrogen donors. The *R*,*R*,*R*,*R* configuration affords the Δ isomer while that of the *S*,*S*,*S*,*S* form produces the Λ isomer. Complex **3** crystallised in non-centrosymmetric space group *Pnn*2 and the absolute configuration of the enantiomorph present in the crystal structure was determined unequivocally as being *S*,*S*,*S*,*S* and the Λ isomer The helical chirality can be characterised by the average $\beta$ angle, calculated with two *cis* torsion angles defined by the pyridine nitrogen atoms and the adjacent carbon atoms [*e.g.* C(3),N(4),N(14), C(15) and C(5),N(4),N(14),C(13) in **3**, **4** and **5**]. Complex **3** with *S*,*S*,*S*,*S* stereochemistry gives Δ helical topology with a $\beta$ angle of −93.6(11)°.

For the *R*,*R*,*R*,*R* form, a symmetric $\beta$ angle of 93.6(11)° would be observed. The remaining four complexes reported here, as well as the other related ones listed in the Table 5 have centrosymmetric space groups and, consequently, their crystals contain a racemic mixture of enantiomorphs with $\pm\beta$ angles. The $\beta$ angles given in Table 5 correspond to the *S*,*S*,*S*,*S* form.

### NMR spectroscopic data in solution

Crystals of the $Zn^{2+}$, $Cd^{2+}$ and $Pb^{2+}$ complexes with [20]$py_2N_4$ suitable for X-ray diffraction could not be obtained, however, the $^1$H and $^{13}$C NMR spectra of these complexes in $D_2O$ were recorded (Table 7) and gave some indications of their structures in solution. The complexes of [18]$py_2N_4$ with $Zn^{2+}$ [9] and with $Cd^{2+}$, $Mg^{2+}$, $Ca^{2+}$, $Sr^{2+}$, $Pb^{2+}$ and $Hg^{2+}$ [10] in DMSO-$d_6$ and $D_2O$ have been previously studied by NMR. We have extended the range of complexes to include those of [20]$py_2N_4$ and, by using variable temperature NMR, have achieved complete elucidation of the spectra of [18]$py_2N_4$ with zinc, cadmium and lead in $D_2O$. The spectral assignments correspond to the labelling shown in Scheme 1.

The $^{13}$C NMR spectra of the complexes of $Zn^{2+}$, $Cd^{2+}$ and $Pb^{2+}$ with [20]$py_2N_4$ exhibit only six resonances, indicating their high symmetry. Thus, both the [18]$py_2N_4$ complexes (which show five resonances),[9,10] and the [20]$py_2N_4$ complexes adopt octahedral geometry achieved by meridional twisting of the macrocycle around the metal, as found in the X-ray crystal structures of the $Co^{3+}$, $Ni^{2+}$ and $Cu^{2+}$ complexes (Fig. 1–3).

The $^1$H NMR spectra of the zinc complex of [20]$py_2N_4$ show seven resonances [Table 7, Fig. 4(a)] over the range of temperatures studied: a triplet and a doublet for the $H_a$ and $H_b$ protons of the pyridine ring, two doublets for the AB spin system of the geminal $H_d$ and $H_{d'}$ protons, two multiplets corresponding to the $H_f$ and $H_{f'}$ protons, which form an AA′BB′ spin system, and one quintuplet corresponding to the $H_g$ protons. The $^1$H NMR spectrum of the $Cd^{2+}$ complex of [20]$py_2N_4$ is similar to that seen for $[Zn([20]py_2N_4)]^{2+}$ [Table 7, Fig. 4(b)], but all resonances, except for the $H_a$ and $H_b$ protons, become broader with increasing temperature, and cadmium satellites ($^{111/113}$Cd, $I$ = 1/2, 25% natural abundance) can be observed for one of the the $H_{d,d'}$ geminal protons. The NMR spectrum of the $Pb^{2+}$ complex of [20]$py_2N_4$, in contrast to the Zn and Cd complexes, shows chemical and magnetic equivalence for the $H_{d,d'}$ and $H_{f,f'}$ protons [Table 7, Fig. 4(c)].[31] Even so, a 15 Hz coupling between the $H_{d,d'}$ protons and $^{207}$Pb ($I$ = 1/2, natural abundance 22.6%) is seen.

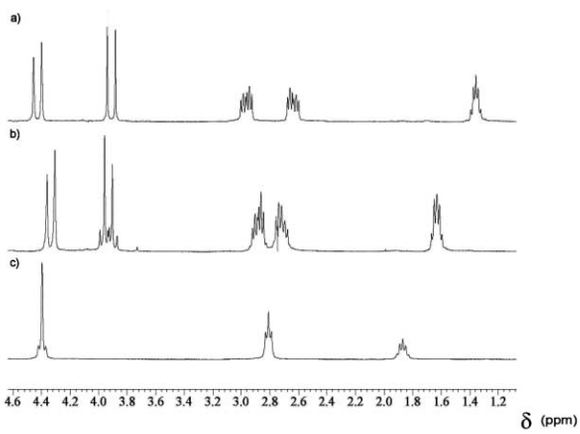


**Fig. 4** $^1$H NMR spectra of $[Zn([20]py_2N_4)]^{2+}$ (a), of $[Cd([20]py_2N_4)]^{2+}$ (b), and of $[Pb([20]py_2N_4)]^{2+}$ (c) in $D_2O$ at 300 K recorded using a 300 MHz spectrometer.

For the three [20]$py_2N_4$ complexes, the resonance corresponding to the amine protons ($H_e$) is not observed, which indicates complete exchange of NH for ND in $D_2O$. The $^1$H NMR spectrum of the $Zn^{2+}$ complex of [18]$py_2N_4$ was acquired and the presence of a broad resonance for $H_e$ was confirmed,[8] indicating no or only partial exchange of NH for ND in $D_2O$. Using a 500 MHz instrument at 300 K, it was possible to observe the splitting of $H_{d,d'}$ resonances due to the proton $H_e$ in $[Zn([18]py_2N_4)]^{2+}$ in $D_2O$ (see Fig. S2, ESI). Indeed, the resonance corresponding to the $H_{d,d'}$ protons, which appears as a singlet in the free ligand, has an ABX splitting pattern, appearing as two pairs of well-defined doublets. The geminal coupling was found to be 17.06 Hz, and the vicinal couplings $^3J$ ($H_d$-$H_e$) = 6.05 and $^3J$ ($H_{d'}$-$H_e$) = 4.03 Hz. The $H_{f,f'}$ protons in $[Zn([18]py_2N_4)]^{2+}$ are coupled to each other and also to $H_e$, forming an AA′BB′XX′ spin system. However, at 300 K, the $H_e$ resonance is only detectable by integration, as it is completely hidden by one of the doublet pairs corresponding to the $H_{d,d'}$ protons. A decrease in temperature (to 290 K or lower) shifts the $H_e$ resonance to lower field, allowing it to be observed (Fig. S2, ESI). For the

**Table 7** $^{1}H$ and $^{13}C$ NMR data for [18]$py_2N_4$ and [20]$py_2N_4$, and their $Zn^{2+}$, $Cd^{2+}$ and $Pb^{2+}$ complexes in $D_2O$ at 300 K ($\delta$, ppm).[a] For the atom labelling, see Scheme 1

| Compound | pD[a] | Nucleus | $H_a$ | $H_b$ | $C_c$ | $H_{dd'}$ | $H_e$ | $H_{ff'}$ | $H_g$ |
|---|---|---|---|---|---|---|---|---|---|
| [18]$py_2N_4$ | 7.4 | $^{1}H$ | 7.85 (t) | 7.33 (d) | — | 4.01 (s) | — | 2.96 (s) | — |
| | | $^{13}C$ | 138.6 | 122.3 | 156.0 | 52.3 | — | 46.2 | — |
| [Zn([18]$py_2N_4$)]$^{2+}$ | 7.4 | $^{1}H$ | 8.31 (t, $J$ = 7.7) | 7.74 (d, $J$ = 7.7) | — | 4.66, 4.61 (dd, $J$ = 6.05, 17.06) | 4.27 (s, br) | 3.17 (m) | — |
| | | | | | | 4.24, 4.29 (dd, $J$ = 4.03, 17.06) | | 2.59 (m) | |
| | | $^{13}C$ | 144.1 | 125.1 | 156.8 | 52.6 | — | 50.4 | — |
| [Cd([18]$py_2N_4$)]$^{2+}$ | 7.4 | $^{1}H$ | 8.02 (t, $J$ = 7.7) | 7.47 (d, $J$ = 7.7) | — | 4.26 (d, $J$ = 16.9) | — | 3.15 (d, $J$ = 10.5) | — |
| | | | | | | 4.02 (d, $J$ = 16.9, 11.92 Cd) | | 2.38 (d, $J$ = 10.5) | |
| | | $^{13}C$ | 142.0 | 124.5 | 155.4 | 50.5 | — | 49.4 | — |
| [Pb([18]$py_2N_4$)]$^{2+}$ | 7.4 | $^{1}H$ | 7.98 (t, $J$ = 7.7) | 7.47 (d, $J$ = 7.7) | — | 4.30 (br) | — | 3.00 (br) | — |
| | | $^{13}C$ | 143.3 | 125.8 | 156.7 | 51.9 | — | 50.7 | — |
| [20]$py_2N_4$ | 7.7 (8.5) | $^{1}H$ | 7.84 (7.83) (t) | 7.35 (7.34) (d) | — | 4.00 (4.02) (s) | — | 2.76 (2.68) (t) | 1.85 (1.81) (q) |
| | 7.7 | $^{13}C$ | 138.7 | 122.6 | 155.0 | 51.8 | — | 45.3 | 26.3 |
| [Zn([20]$py_2N_4$)]$^{2+}$ | 7.7 | $^{1}H$ | 8.10 (t, $J$ = 7.9) | 7.55 (d, $J$ = 7.8) | — | 4.42, 3.92 (dd, $J$ = 17.1) | — | 2.96, 2.63 (ddd, $J$ = 12.6, 5.6, 5.4) | 1.36 (ddd, $J$ = 5.4) |
| | | $^{13}C$ | 141.5 | 122.3 | 154.4 | 52.4 | — | 52.0 | 24.7 |
| [Cd([20]$py_2N_4$)]$^{2+}$ | 8.5 | $^{1}H$ | 8.03 (t, $J$ = 7.8) | 7.48 (d, $J$ = 7.8) | — | 4.33, 3.93 (dd, $J$ = 16.5, Cd 19.2) | — | 2.86, 2.72 (ddd, $J$ = 12.6, 5.6, 5.1) | 1.63 (ddd, $J$ = 5.7) |
| | | $^{13}C$ | 140.8 | 122.8 | 154.6 | 51.4 | — | 50.2 | 25.1 |
| [Pb([20]$py_2N_4$)]$^{2+}$ | 8.7 | $^{1}H$ | 8.01 (t, $J$ = 7.8) | 7.53 (d, $J$ = 7.8) | — | 4.39 (s br, Pb $J$ = 15.9) | — | 2.81 (t, $J$ = 6.3) | 1.87 (q, $J$ = 6.0) |
| | | $^{13}C$ | 140.1 | 122.9 | 158.7 | 53.6 | — | 45.2 | 25.4 |

[a] Chemical shifts referenced to 3-(trimethylsilyl)propionic acid-$d_4$ sodium salt (0.000 ppm) and $J$ values in hertz.

$Cd^{2+}$ and $Pb^{2+}$ complexes of [18]$py_2N_4$, the exchange of NH for ND in $D_2O$ is complete and the $H_e$ resonance does not appear (Table 7). The doublet at 4.02 ppm in the spectrum of [Cd([18]$py_2N_4$)]$^{2+}$ shows coupling with $^{111/113}Cd$, as seen for [Cd([20]$py_2N_4$)]$^{2+}$. Only one $H_d$–Cd vicinal coupling is seen, due to the H–C–N–Cd dihedral angle being almost 90° for one of the $H_d$ protons, as also seen in the X-ray crystal structure of **8**. Interestingly, the Pb complex of [18]$py_2N_4$ shows two broad lines for the $H_{d,d'}$ and $H_{f,f'}$ protons, which is consistent with $\delta/\lambda$ conformational interconversion of the ethylenic linkage.[10] The fact that the NH/ND exchange does not occur for the $H_e$ protons in [Zn([18]$py_2N_4$)]$^{2+}$ is indicative of unusual structural rigidity and inertness toward metal exchange for this complex in solution.[9]

For the metal complexes of [18]$py_2N_4$, it was observed that as the size of the metal ion increases from $Zn^{2+}$ to $Cd^{2+}$, the chemical shift difference between protons $H_d$ and $H_{d'}$ decreases, while that between protons $H_f$ and $H_{f'}$ increases.[10] This effect was confirmed here for the Zn and Cd [18]$py_2N_4$ complexes at 500 MHz. The effect could not be observed in the Pb complex, due to the presence of broad lines. These chemical shift effects are related to the untwisting of the macrocycle to accommodate the larger metal ions causing the $–N_{sp^2}–C_{sp^2}–C_{sp^3}–N_{sp^3}–$ chelate ring to become eclipsed, with the consequent decrease of the corresponding torsion angle and an increase in the $–N_{sp^3}–C–C–N_{sp^3}–$ torsion angle. This is confirmed in the X-ray structures of [Zn([18]$py_2N_4$)]$^{2+}$ (**7**) and [Cd([18]$py_2N_4$)]$^{2+}$ (**8**) where the $–N_{sp^2}–C_{sp^2}–C_{sp^3}–N_{sp^3}–$ torsion angles are 26.9 and 25.3/25.0°, respectively, and those formed by $–N_{sp^3}–C–C–N_{sp^3}–$ are 63.5 and 69.8°, respectively.[10]

A decrease in chemical shift difference between $H_{d,d'}$ protons as the metal size increases was also observed for the [20]$py_2N_4$ complexes (the Pb complex has magnetically equivalent $H_{d,d'}$ protons). The $H_{f,f'}$ protons, however, showed different behaviour, with a decreasing difference seen for increasing metal size. This suggests that as the macrocycle untwists to accommodate a larger metal ion, the environments of the two geminal $H_{f,f'}$ protons become similar. Interestingly, the average chemical shift for the $H_{f,f'}$ protons does not change with metal ion size. The $H_{gg'}$ protons become more deshielded with increasing size.

Comparing chemical shifts between [18]$py_2N_4$ and [20]$py_2N_4$ complexes for the same metal, it can be seen that the difference between the $H_{f,f'}$ protons for Zn complexes is larger for [18]$py_2N_4$ (0.58 ppm) than for [20]$py_2N_4$ (0.33 ppm). The $H_{d,d'}$ protons, however, show a larger shift difference for [20]$py_2N_4$ (0.50 ppm) than for [18]$py_2N_4$ (0.37 ppm). The same trend is seen for the chemical shift differences between the $H_{d,d'}$ and $H_{f,f'}$ protons in the Cd complexes of [18]$py_2N_4$ and [20]$py_2N_4$ (Table 7), which suggests that as the ring size is increased, the shielding of the $H_{f,f'}$ protons becomes more similar (the effect being more pronounced for Cd than for Zn), while the shielding of the $H_{d,d'}$ protons become more different.

The structures of the Zn and Cd complexes of [20]$py_2N_4$ in gas phase were simulated by MM calculations using the crystal structure of **4** and replacing Ni with Zn or Cd. Then, these trial models were optimised (see Experimental section), with $M–N_{sp^2}$ and $M–N_{sp^3}$ constrained at 2.120 and 2.161 Å for Zn, and 2.395 and 2.360 Å for Cd, which are averaged distances from X-ray structures deposited on the CSD.[14] The minimised structure of [Zn([20]$py_2N_4$)]$^{2+}$ shows a distorted octahedral geometry with a $\beta$ angle of −121° (*ca.* 6° less than those of **4** or **5**) and the $–N_{sp^2}–C_{sp^2}–C_{sp^3}–N_{sp^3}$ torsion angles are 13.8 and 24.6°. As expected, the Cd structure is significantly more distorted, having a $\beta$ angle of −106° (which is between the reported values for **3** and **4** or **5**) and two different $N_{sp^2}–C_{sp^2}–C_{sp^3}–N_{sp^3}–$ torsion angles of 1.4 and 29.1°. These preliminary calculations show that, for the complexes of [20]$py_2N_4$, it is difficult to establish a direct correlation between the $^{1}H$ NMR chemical shift of $H_{d,d'}$ and $H_{f,f'}$ with the $–N_{sp^2}–C_{sp^2}–C_{sp^3}–N_{sp^3}–$ and $–N_{sp^3}–C–C–N_{sp^3}$

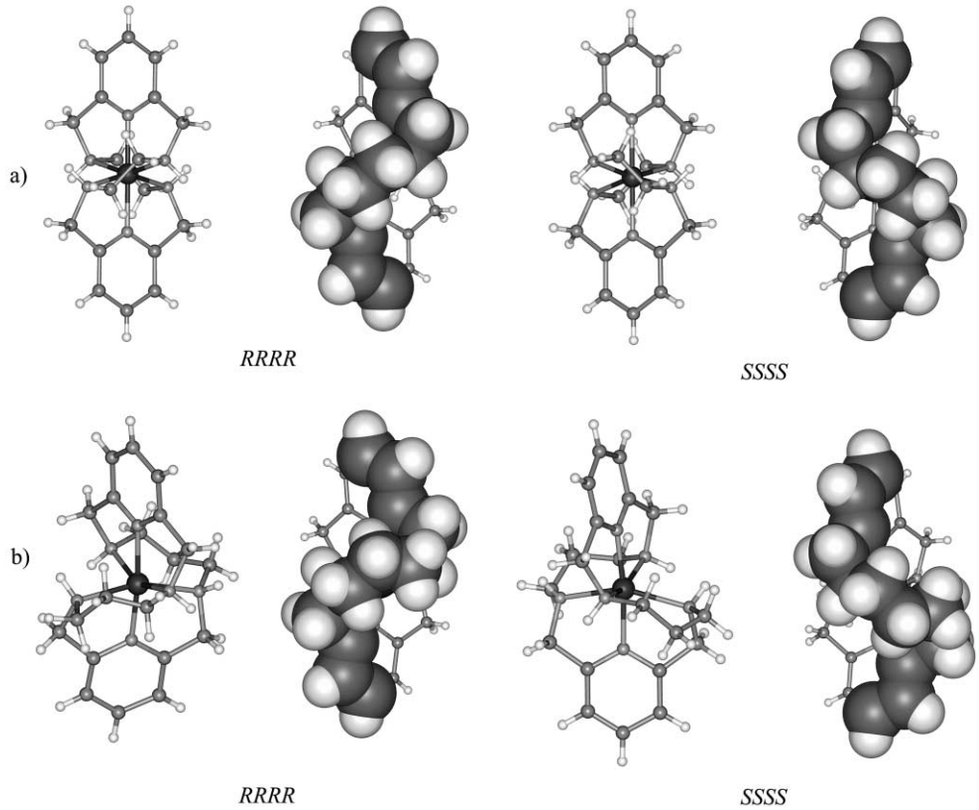


**Fig. 5** Molecular diagrams (CPK and ball–stick representations) illustrating the helical chirality of the *R*,*R*,*R*,*R* and *S*,*S*,*S*,*S* enantiomorphic forms for $[18]py_2N_4$ and $[20]py_2N_4$ octahedral complexes: (a) $[Ni([18]py_2N_4)]^{2+}$; (b) $[Ni([20]py_2N_4)]^{2+}$.

endocyclic torsion angles, respectively, as was done for the complexes of $[18]py_2N_4$. This was expected due to the flexibility of $[20]py_2N_4$ macrocycle.

## Conclusions

The structural data presented in this work and summarised in Tables 5 and 7 show that the $[18]py_2N_4$ and $[20]py_2N_4$ macrocycles fold in a helical shape in order to encapsulate metal ions in a hexaco-ordinate environment. The high stability constants of the complexes of the transition and post-transition metal ions also indicate co-ordination of all the donor atoms of both ligands. The $[18]py_2N_4$ and $[20]py_2N_4$ helical topologies on metal complexes are compared in Fig. 5 for nickel species **1** and **4**. The molecular dimensions associated with metal co-ordination sphere and molecular mechanics calculations show that both macrocycles have enough flexibility to encapsulate metal ions with different sizes and also demonstrate that the insertion of the metal into the macrocyclic cage occurs *via* a recognition system based on the best fit between macrocyclic cage and metal ion size. Thus, a smaller ion such as $Co^{3+}$ fits better than $Cu^{2+}$ or $Ni^{2+}$ into the $[20]py_2N_4$ cage, as indicated by the degree of tetrahedral distortion reported for these two complexes. On average, the distortion found for the cobalt complex **3** is *ca.* one-half of that found for the copper (**5**) and nickel (**4**) complexes.

The same structural trends are observed for $[18]py_2N_4$ complexes and the tetrahedral distortions, as would be expected, are consistent with the stereoelectronic requirements of the metal ions, following the order $Cd^{2+} > Zn^{2+} > Cu^{2+} > Ni^{2+}$.

On other hand, the macrocyclic topology can be characterised by the $\beta$ torsion angle, defined above, which shows a straightforward relationship with the helicity of the macrocycle. The value of this parameter aids understanding of the process whereby the metal is inserted into the macrocyclic cage.

In fact, the $[18]py_2N_4$ complexes **1**, **2** and **7** contain comparable $|\beta|$ angles and, consequently, identical helicities. The $|\beta|$ angle is reduced by *ca.* 15° in the $Cd^{2+}$ complex **8**, suggesting that the macrocycle unfolds around the helical axis, with a concomitant expansion of the cage, in order to accommodate this larger metal ion.

The $Cu^{2+}$ and $Ni^{2+}$ complexes of $[20]py_2N_4$ display also identical helicities, with $|\beta|$ angles of 115.3(7)° in **4** and 115.0(5)° in **5** (Table 5), which decreases to 91.6° for the $Co^{3+}$ complex **3**. So, an unfolding process of the $[20]py_2N_4$ macrocycle occurs from $Cu^{2+}$ or $Ni^{2+}$ to $Co^{3+}$ complexes, which is identical to that described for the $[18]py_2N_4$ complexes (from $Ni^{2+}$, $Cu^{2+}$ and $Zn^{2+}$ to $Cd^{2+}$), but, in this case, in order to accommodate a smaller metal ion, such as $Co^{3+}$.

Finally, the $Cu^{2+}$ and $Ni^{2+}$ complexes of both macrocycles show comparable tetrahedral distortions, but present obviously different helicities. The $[20]py_2N_4$ macrocycle is more twisted around the metal by *ca.* 10° more than the $[18]py_2N_4$ macrocycle. In other words, the insertion of two $CH_2$ units increases the helicity of the macrocyclic topology in order to satisfy the stereoelectronic requirements of the metal centre (see Fig. 5).

## Experimental

Microanalyses were carried out by the ITQB Microanalytical Service. IR spectra were recorded from KBr pellets on a UNICAM Mattson 7000 spectrometer.

### Reagents

All the chemicals were of reagent grade and used as supplied without further purification. The reference used for the $^1H$ NMR measurements in $D_2O$ was 3-(trimethylsilyl)propanoic acid-$d_4$-sodium salt and, in $CDCl_3$, the solvent itself. For $^{13}C$ NMR in $D_2O$ spectra, dioxane was used as the internal reference.

**CAUTION**: although no problems were encountered in this work, perchlorates in presence of organic matter are potentially explosive and should be prepared and handled in small quantities.

2,6-Pyridinedimethanol was obtained from Aldrich and 2,6-pyridinedicarbaldehyde was prepared by the published method.[26]

3,6,14,17,23,24-hexaazatricyclo[17.3.1.1$^{8,12}$]tetracosa-1(23),8,10,12(24),19,21-hexaene ([18]py$_2$N$_4$) was prepared by the procedure described by Jackels *et al.*,[8] but obtained as an yellow solid in the form of the pure amine and characterised in this form. Yield: 65%. M.p. 141–142 °C. $^1$H NMR ($CDCl_3$): $\delta$ 2.803 (s, 8 H, –HNC$H_2$CH$_2$NH–), 3.857 (s, 8 H, –HNC$H_2$py), 7.040 (d, 4 H, 3,5-py) and 7.54 (t, 2 H, 4-py); $^{13}$C NMR ($CDCl_3$): $\delta$ 49.0 (–HNCH$_2$CH$_2$NH–), 54.7 (–HN*C*H$_2$py), 120.8 (3,5-*C*py), 136.7 (4-*C*py) and 159.0 (*o*-*C*py). Found: C, 62.4; H, 8.28; N, 24.6; calc. for $C_{18}H_{26}N_6\cdot H_2O$: C, 62.77; H, 8.19; N, 24.40%. IR (KBr pellets, cm$^{-1}$): $\nu_{O-H}$ 3449 (br); $\nu_{N-H}$ 3333 (m); $\nu_{C-H}$ 2909–2820 (m); $\nu_{N-H}$ 2321 (w); $\nu_{C=C}$, $\nu_{C=N}$ 1686 (w), 1574 (s); 1468 (s); 1435 (s); $\nu_{C-H}$ 1346 (w), 1221 (m), 1119 (s), 993–789 (vs).

3,7,15,19,25,26-hexaazatricyclo[19.3.1.1$^{9,13}$]hexacosa-1(25),9,11,13(26),21,23-hexaene ([20]py$_2$N$_4$) was prepared as described in the literature,[11] but obtained in the form of the pure amine as a white powder. Yield: 82%. M.p. 105–108 °C. $^1$H NMR ($CDCl_3$): $\delta$ 1.717 (q, 4 H, –CH$_2$C$H_2$CH$_2$–), 2.612 (m, 8 H, –HNC$H_2$CH$_2$C$H_2$NH–), 2.907 (s, 8 H, NC$H_2$py), 7.040 (d, 4 H, 3,5-py) and 7.521 (t, 4 H, 4-py); $^{13}$C NMR ($CDCl_3$): $\delta$ 29.9 (–CH$_2$*C*H$_2$CH$_2$–), 47.1 (–HN*C*H$_2$CH$_2$*C*H$_2$NH–), 54.2 (–HN-*C*H$_2$py), 120.7 (3,5-*C*py), 136.6 (4-*C*py) and 158.5 (*o*-*C*py). Found: C, 58.64; H, 8.91; N, 20.63; calc. for $C_{20}H_{30}N_6\cdot 3H_2O$: C, 58.80; H, 8.88; N, 20.57%. IR (KBr pellets, cm$^{-1}$): $\nu_{O-H}$ 3449 (br); $\nu_{N-H}$ 3333 (m); $\nu_{C-H}$ 2922–2837 (m); $\nu_{N-H}$ 2330 (br); $\nu_{C=C}$, $\nu_{C=N}$ 1680 (s), 1593 (s); 1462 (s); 1435 (s); $\nu_{C-H}$ 1342 (w), 1263 (w), 1117 (s), 995–793 (s).

Five equiv. of $HNO_3$ were added to aqueous solutions of the amines [18]py$_2$N$_4$ and [20]py$_2$N$_4$ for the potentiometric and spectrophotometric studies.

**Synthesis of [Ni([18]py$_2$N$_4$)](ClO$_4$)$_2$·2CH$_3$CN (1).** An aqueous solution of Ni(ClO$_4$)$_2$·6H$_2$O (0.1 mmol, 0.0366 g) was added to a stirred solution of [18]py$_2$N$_4$ (0.1 mmol, 0.0326 g) dissolved in the minimum volume of water (≈ 2 cm$^3$), and the mixture was stirred for 0.5 h. The solvent was removed under vacuum and the mixture dissolved in ethanol. The precipitate formed was filtered off and the solvent removed again. The pure complex was dissolved in a mixture of methanol and acetonitrile (5 : 1). Pale blue crystals were formed after five days by slow evaporation of the solvent at room temperature. Yield ≈85%. Found: C, 39.5; H, 4.7; N, 16.8; calc. for $C_{22}H_{32}Cl_2N_8NiO_8$: C, 39.72; H, 4.85 N, 16.84%.

**Synthesis of [Cu([18]py$_2$N$_4$)](ClO$_4$)$_2$·2CH$_3$CN (2).** An aqueous solution of Cu(ClO$_4$)$_2$·6H$_2$O (0.122 mmol, 0.0452 g) was added to a stirred solution of [18]py$_2$N$_4$ (0.122 mmol, 0.04 g) dissolved in the minimum volume of water (≈ 1 cm$^3$). Then, 0.04 g (0.244 mmol) of $NH_4PF_6$ were added, the pH of the solution increased to 5.5 by addition of an aqueous solution of KOH (0.1 mol dm$^{-3}$) and the mixture was stirred for 0.5 h. The solvent was evaporated under vacuum and the mixture dissolved in ethanol. The precipitate formed was filtered off and the solvent removed again. The pure complex was dissolved in a mixture of ethanol and acetonitrile (1 : 1). Blue–turquoise needles were formed after three weeks by slow evaporation of the solvent at room temperature. Yield ≈ 85%. Found: C, 39.2; H, 4.9; N, 16.6; calc. for $C_{22}H_{32}Cl_2CuN_8O_8$: C, 39.44; H, 4.81; N, 16.72%.

**Synthesis of [Co([20]py$_2$N$_4$)][Co(H$_2$O)$_6$]$_{0.5}$(SO$_4$)$_2$ (3).** An aqueous solution of $CoSO_4\cdot 7H_2O$ (0.0675 mmol, 0.0239 g) was added to a stirred solution of [20]py$_2$N$_4$ (0.05 mmol, 0.0177 g) dissolved in the minimum volume of water (≈ 1 cm$^3$). The pH of the solution was increased to 7.3 by addition of an aqueous solution of KOH (0.1 mol dm$^{-3}$) and the mixture was stirred for 0.5 h. Then, the solvent was evaporated under vacuum, the inorganic matter separated by addition of methanol and the mixture finally dissolved in methanol–tetrahydrofuran (10 : 1). Orange crystals were formed after about two months at 8 °C. Yield ≈ 40%.

**Synthesis of [Ni([20]py$_2$N$_4$)](ClO$_4$)$_2$ (4).** An aqueous solution of Ni(ClO$_4$)$_2$·6H$_2$O (0.02 mmol, 0.0073 g) was added to a stirred solution of [20]py$_2$N$_4$ (0.01 mmol, 0.00254 g) dissolved in the minimum volume of water (≈ 3 cm$^3$), the pH increased to 7.2 with aqueous KOH solution (0.1 mol dm$^{-3}$) and the mixture was stirred for 1 h. The solvent was removed under vacuum and the mixture dissolved in ethanol. The precipitate formed was filtered off and the solvent removed again. The pure complex was dissolved in acetonitrile. Pale blue crystals were formed after 21 days by slow evaporation of the solvent at room temperature. Yield ≈ 75%. C, 36.23; H, 4.68; N, 12.82; calc. for $C_{20}H_{30}Cl_2N_6NiO_8\cdot 2H_2O$: C, 36.11; H, 4.85; N, 12.63%.

**Synthesis of [Cu([20]py$_2$N$_4$)](ClO$_4$)$_2$ (5).** This complex was prepared by the procedure used for **4**, using Cu(ClO$_4$)$_2$·6H$_2$O (0.01 mmol, 0.0037 g) and the pH set at 6.5. The slow evaporation of the complex was carried out from a mixture of ethanol and acetonitrile (1 : 3). Intense blue crystals were formed after about one week at room temperature. Yield ≈ 72%. C, 39.1; H, 4.5; N, 13.6; calc. for $C_{20}H_{30}Cl_2CuN_6O_8\cdot 2H_2O$: C, 39.25; H, 4.28; N, 13.70%.

### Potentiometric measurements

**Reagents and solutions.** Metal ion solutions were prepared at concentrations of about 0.025 mol dm$^{-3}$ from the nitrate salts of the metals (analytical grade) with demineralised water (obtained by a Millipore/Milli-Q system) and were standardised as described.[26,32] Carbonate-free solutions of the titrant, KOH, were obtained, maintained and discarded as described.[26,32]

**Equipment and work conditions.** The equipment used was described previously.[26,32] The temperature was kept at 25.0 ± 0.1 °C; atmospheric $CO_2$ was excluded from the cell during the titration by passing purified nitrogen across the top of the experimental solution in the reaction cell. The ionic strength of the solutions was kept at 0.10 mol dm$^{-3}$ with $KNO_3$.

**Measurements.** The [H$^+$] of the solutions was determined by the measurement of the electromotive force of the cell, $E = E'^\circ + Q\log [H^+] + E_j$. $E'^\circ$, $Q$, $E_j$ and $K_w = ([H^+][OH])$ were obtained as described previously.[26,32] The term pH is defined as $-\log [H^+]$. The value of $K_w$ was found to be equal to $10^{-13.80}$ mol$^2$ dm$^{-6}$.

The potentiometric equilibrium measurements were carried out using 20.00 cm$^3$ of ≅$2.50 \times 10^{-3}$ mol dm$^{-3}$ ligand solutions diluted to a final volume of 30.00 cm$^3$, in the absence of metal ions and in the presence of each metal ion for which the $C_M : C_L$ ratios were 1 : 1 and 2 : 1. A minimum of two replicate measurements was taken.

The equilibrium for the complex formation reactions was reached quickly for most complexes. The same values of the stability constants were obtained either using the direct or the back titration curves. For the Ni$^{2+}$, Zn$^{2+}$ and lanthanides complexes of both ligands, slow reactions were observed and, in these cases, batch titrations were performed. The solutions of the Cu$^{2+}$ and Ni$^{2+}$ complexes of [18]py$_2$N$_4$ and [20]py$_2$N$_4$ for spectrophotometric measurements (batch method) were prepared in individual vials (adding equimolar amounts of metal and ligand, sufficient potassium nitrate for a 0.1 mol dm$^{-3}$ solution, water to the appropriate volume and the amount of base required to achieve a specific pH) and allowed to equilibrate for 15 to 30 days before the last reading of potential or absorbance.

**Calculation of equilibrium constants.** Protonation constants, $K_i^H = [H_iL]/[H_{i-1}L][H]$, were calculated by fitting the potentiometric data obtained for the free ligand to the HYPERQUAD program.[17] Stability constants of the various species formed in solution were obtained from the experimental data (from potentiometric or spectrophotometric titrations) corresponding to the titration of solutions of different metal ion to ligand ratios, also using the HYPERQUAD program. The initial computations were obtained in the form of overall stability constants, $\beta_{M_mH_hL_l} = [M_mH_hL_l]/[M]^m[L]^l[H]^h$

Only mononuclear species, ML, MHL, $MH_2L$ and M(−H)L [$\beta_{M(-H)L} = \beta_{MLOH} \times K_w$] were found. Differences, in log units, between the values $\beta_{MHL}$ [or $\beta_{M(-H)L}$] and $\beta_{ML}$ provide the stepwise protonation reaction constants, shown in Table 1. The errors quoted are the standard deviations of the overall stability constants given directly by the program for the input data, which include all the experimental points of all titration curves. The standard deviations of the stepwise constants were determined by the normal propagation rules.

The protonation constants were obtained from >250 experimental points (5 titration curves) for [18]$py_2N_4$ and from >150 experimental points (3 titration curves) for [20]$py_2N_4$. The stability constants for each metal ion were determined from 100 to 150 experimental points (2 to 4 titration curves). All the points of a titration were used in the calculations except those obtained with a simultaneous formation of a precipitate, which generally do not stabilise. In these cases, spectrophotometric titrations were performed ($Ni^{2+}$ and $Cu^{2+}$ both with [18]$py_2N_4$ and [20]$py_2N_4$), and these spectrophotometric data were then coupled together with the potentiometric data and fitted to the calculated results with the same model with the Hyperquad program.[17] The constants for those complexes were determined with at least two potentiometric titrations at different M : L ratios and one or two spectrophotometric titrations using 20 or more different wavelengths for each pH value.

### Spectroscopic studies

$^1H$ and $^{13}C$ NMR spectra were recorded on Bruker CXP-300 or DRX-500 spectrometers. Solutions of the ligands and complexes in $D_2O$ for spectroscopy (≈ 0.01 mol $dm^{-3}$) were made up and the pD was adjusted by addition of DCl or $CO_2$-free KOD with an Orion 420A instrument fitted with a combined Ingold 405M3 microelectrode. The −log [$D^+$] was measured directly in the NMR tube, after calibration of the microelectrode with buffered aqueous solutions. The final pD was calculated from pD = pH* + 0.40.[33] The value of pH* corresponds to the reading of the pH meter previously calibrated with two standard aqueous buffers at pH 4 and 7. Electronic spectra were measured with a UNICAM model UV-4 spectrophotometer for UV-vis, using aqueous solutions of the complexes prepared by the addition of the metal ion (in the form of nitrate salt) to the ligand at the appropriate pH value.

### Crystallography

A summary of the crystallographic data, together with data collection and the refinement details for [Ni([18]$py_2N_4$)]$(ClO_4)_2$·$2CH_3CN$ (**1**), [Cu([18]$py_2N_4$)]$(ClO_4)_2$·$2CH_3CN$ (**2**), and [Co([20]$py_2N_4$)][$Co(H_2O)_6$]$_{0.5}(SO_4)_2$·$CH_3OH$·$4H_2O$ (**3**), [Ni([20]$py_2N_4$)]$(ClO_4)_2$ (**4**) and [Cu([20]$py_2N_4$)]$(ClO_4)_2$ (**5**) are listed in Table 3. X-Ray data sets for these five compounds were collected on a MAR research image plate system equipped with graphite-monochromated Mo-Kα radiation (0.71073 Å). 95 Frames were measured at 2° intervals using a counting time adequate for the crystal under study. Data analyses were performed with the XDS program.[34] In general, the crystals presented poor diffraction patterns, leading to slightly high $R$ values. No absorption correction was applied to the intensities. The structures were solved by direct methods and refined by full-matrix least-squares against $F^2$ using SHELXS and SHELXL from the SHELX97 package.[35]

In complex **1**, the unique $ClO_4^-$ that comprised the asymmetric unit was found to be disordered. Two sets of tetrahedral oxygen atoms were considered and were refined with occupation factors of $x$ and $1 - x$, with $x$ refined to 0.61(1). In the disordered anion, the chlorine atom was refined anisotropically and the oxygen atoms using group isotropic thermal parameters. The dimensions of the two tetrahedra were constrained during the refinement. In complexes **4** and **5**, one of the two $ClO_4^-$ anions was also located over two positions and an equivalent model was used to describe the disorder. Refined occupancies ($x$, $1 - x$) for oxygen atoms were 0.46(1), 0.54(1) in **4** and 0.56(1), 0.44(1) in **5**. In both cases, the oxygen atoms were refined with individual isotropic thermal parameters. In the ordered $ClO_4^-$ anion, all atoms were refined using anisotropic thermal displacements. The complex cations, as well as the $CH_3CN$ solvent molecules, in **1** and **2** were refined with anisotropic thermal displacements.

The hydrogen atoms bonded to the carbon and nitrogen atoms were inserted in geometric positions while the hydrogens of the water molecules in complex **3** were localised from difference Fourier maps and refined with O–H and H ··· H distances constrained *via* the DFIX tool in order to give an ideal H–O–H angle of 104.5°. All atomic hydrogen positions were refined, giving isotropic thermal parameter equal to 1.2 times those of the atoms to which they were bonded.

The absolute configuration of the structure of the complex cation **3** in the space group *Pnn*2 was determined unequivocally from X-ray data. The trial model with *R*,*R*,*R*,*R* stereochemistry gave for $R$ and $R_w$ (all data) values of 0.1352 and 0.1881, respectively, which are slightly reduced to 0.1347 and 0.1870, when the configuration was inverted to *S*,*S*,*S*,*S*. Furthermore, the Flack parameter is 0.07(4) for *R*,*R*,*R*,*R* and 0.01(4) for the *S*,*S*,*S*,*S* form, as expected for the correct configuration.[36] But the Flack parameter ought to be close to 1.0 for the wrong *R*,*R*,*R*,*R* form.

ORTEP diagrams were drawn with PLATON[37] and WEBLAB VIEWER[38] graphical software packages.

CCDC reference numbers 185052–185056.

See http://www.rsc.org/suppdata/dt/b2/b204189h/ for crystallographic data in CIF or other electronic format.

### Molecular mechanics calculations

Molecular mechanics calculations were carried out using the universal force field[30] within the Cerius$^2$ software.[39] The X-ray structures of the nickel cations **1** and **4** were taken as starting models. The strain energies for hexaco-ordinate [M([18]$py_2N_4$)] and [M([20]$py_2N_4$)] models were calculated using a similar methodology to that described before, although slightly modified.[28,29] The metal co-ordination environment was allowed to relax without any constraints on the angles subtended at the metal centre. All four M–N distances were fixed *via* the Force Field Editor tool, using large force constants of 7000 kcal $mol^{-1}$ $Å^{-2}$ for the stretching terms. A difference of 0.1 Å between M–$N_{sp^3}$ and M–$N_{sp^2}$ distances was taken into account in all MM calculations, since this is observed in most of the X-ray structures of metal transition complexes of macrocycles containing pyridine moieties. Then, the energy profiles of the conformers relative to M–N distances were obtained by concomitantly changing the M–$N_{sp^3}$ and M–$N_{sp^2}$ distances successively at 0.05 Å intervals over the range 1.7 to 2.5 Å. Partial charges were not included because they were difficult to calculate accurately and only have marginal impact on relative strain energies in metal complexes.

## Acknowledgements

The authors acknowledge financial support from Fundação para a Ciência e Tecnologia (FCT) and POCTI, with co-participation of the European Community fund FEDER (Project no. POCTI/1999/QUIM/35396).

## References


1 M. Mitewa and P. R. Bontchev, *Coord. Chem. Revs.*, 1994, **135/136**, 129.
2 G. H. Searle, *Bull. Chem. Soc. Jpn.*, 1989, **62**, 4021.
3 A. Bianchi, M. Micheloni and P. Paoletti, *Coord. Chem. Rev.*, 1991, **130**, 17.
4 J. Comarmond, P. Plumeré, J. M. Lehn, Y. Agnus, R. Louis, R. Weiss, O. Kahn and I. Morgenstern-Badarau, *J. Am. Chem. Soc.*, 1982, **104**, 6330.
5 A. Bencini, A. Bianchi, P. Dapporto, E. Garcia-España, M. Micheloni, P. Paoletti and P. Paoli, *J. Chem. Soc., Chem. Commun.*, 1990, 1382.
6 A. McAuley, T. W. Whitcombe and M. J. Zaworotko, *Inorg. Chem.*, 1991, **30**, 3513.
7 G. R. Newkome, V. K. Majestic and F. R. Fronczek, *Inorg. Chim. Acta*, 1983, **77**, L47.
8 G. L. Rothermel, Jr., L. Miao, A. L. Hill and S. C. Jackels, *Inorg. Chem.*, 1992, **31**, 4854.
9 L. H. Bryant, Jr., A. Lachgar, K. S. Coates and S. C. Jackels, *Inorg. Chem.*, 1994, **33**, 2219.
10 L. H. Bryant, Jr., A. Lachgar and S. C. Jackels, *Inorg. Chem.*, 1995, **34**, 4230.
11 K. I. Dhont, G. G. Herman, A. C. Fabretti, W. Lippens and A. M. Goeminne, *J. Chem. Soc., Dalton Trans.*, 1996, 1753.
12 B. Nieslanik, E. N. Duesler, L. Miao, S. C. Jackels and R. T. Paine, *Acta Crystallogr., Sect C*, 1996, **52**, 205.
13 K. I. Dhont, W. Lippens, G. Herman and A. M. Goeminne, *Bull. Soc. Chim. Belg.*, 1992, **102**, 1061.
14 F. H. Allen and O. Kennard, *Chem. Des. Autom. News*, 1993, **8**, 31.
15 F. Arnaud-Neu, M. Sanchez and M. J. Schwing-Weill, *Helv. Chim. Acta*, 1985, **68**, 840.
16 J. Costa, R. Delgado, M. G. B. Drew and V. Félix, unpublished results.
17 P. Gans, A. Sabatini and A. Vacca, *Talanta*, 1996, **43**, 1739.
18 (*a*) R. M. Smith, A. E. Martell and R. J. Motekaitis, *NIST Critical Stability Constants of Metal Complexes Database*, U.S. Department of Commerce, Gaithersburg, MA, 1993; (*b*) L. D. Pettit and H. K. J. Powell, IUPAC Stability Constants Database, Academic Software, Timble, UK, 1993.
19 M. Kodama, E. Kimura and S. Yamaguchi, *J. Chem. Soc., Dalton Trans.*, 1980, 2536.
20 W. Szczepaniak, B. Juskowiak and W. Ciszewska, *Inorg. Chim. Acta*, 1988, **147**, 261.
21 A. Bencini, A. Bianchi, M. Micheloni, P. Paoletti, E. Garcia-España and M. A. Niño, *J. Chem. Soc., Dalton Trans.*, 1991, 1171.
22 A. Bencini, A. Bianchi, P. Dapporto, E. Garcia-España, M. Micheloni and P. Paoletti, *Inorg. Chem.*, 1989, **28**, 1188.
23 A. Bencini, A. Bianchi, M. Castelló, M. Di Vaira, J. Faus, E. Garcia-España, M. Micheloni and P. Paoletti, *Inorg. Chem.*, 1989, **28**, 347.
24 A. Andrés, A. Bencini, A. Carachalios, A. Bianchi, P. Dapporto, E. Garcia-España, P. Paoletti and P. Paoli, *J. Chem. Soc., Dalton Trans.*, 1993, 3507.
25 M. Kodama, T. Koike, A. Mahatma and K. Kimura, *Inorg. Chem.*, 1991, **30**, 1270.
26 J. Costa and R. Delgado, *Inorg. Chem.*, 1993, **32**, 5257, and references cited therein.
27 R. Machida, E. Kimura and M. Kodama, *Inorg. Chem.*, 1983, **22**, 2055.
28 J. Costa, R. Delgado, M. G. B. Drew, V. Félix, R. T. Henriques and J. C. Waerenborgh, *J. Chem. Soc., Dalton Trans.*, 1999, 3253.
29 V. Félix, J. Costa, R. Delgado, M. G. B. Drew, M. T. Duarte and C. Resende, *J. Chem. Soc., Dalton Trans.*, 2001, 1462.
30 A. K. Rappé, C. J. Casewit, K. S. Colwell, W. A. Goddard III and W. M. Skiff, *J. Am. Chem. Soc.*, 1992, **114**, 10 024.
31 P. A. Baisden, G. R. Choppin and B. B. Garrett, *Inorg. Chem.*, 1977, **16**, 1367.
32 J. Costa, R. Delgado, M. T. Duarte and V. Félix, *Supramol. Chem.*, 2001, **13**, 333.
33 R. Delgado, J. J. R. Fraústo da Silva, M. T. S. Amorim, M. F. Cabral, S. Chaves and J. Costa, *Anal. Chim. Acta*, 1991, **245**, 271.
34 W. Kabsch, *J. Appl. Crystallogr.*, 1988, **21**, 916.
35 G. M. Sheldrick, SHELX-97, Programs for Solution and Refinement of Crystal Structures, University of Göttingen, Germany, 1997.
36 H. D. Flack, *Acta Crystallogr., Sect. A*, 1983, **39**, 876.
37 A. L. Spek, PLATON, A Multipurpose Crystallographic Tool, Utrecht University, The Netherlands, 1999.
38 WEBLAB VIEWER, version 2.01, Molecular Simulations, Inc., San Diego, CA, USA, 1997.
39 Cerius$^2$, version 3.5, Molecular Simulations Inc., San Diego, CA, USA, 1997.